OUKA
Osaka University Knowledge Archive

Title	Osteogenic tailoring of oriented bone matrix organization using on/off micropatterning for osteoblast adhesion on titanium surfaces
Author(s)	Matsuzaka, Tadaaki; Matsugaki, Aira; Ishihara, Kazuhiko et al.
Citation	Acta Biomaterialia. 2025, 192, p. 487-500
Version Type	VoR
URL	https://hdl.handle.net/11094/100380
rights	This article is licensed under a Creative Commons Attribution 4.0 International License.
Note	

Osaka University Knowledge Archive : OUKA

https://ir.library.osaka-u.ac.jp/

Osaka University

Acta Biomaterialia 192 (2025) 487–500

Contents lists available at ScienceDirect

Acta Biomaterialia

journal homepage: www.elsevier.com/locate/actbio

Full length article

Osteogenic tailoring of oriented bone matrix organization using on/off micropatterning for osteoblast adhesion on titanium surfaces

Tadaaki Matsuzaka, Aira Matsugaki *, Kazuhiko Ishihara, Takayoshi Nakano *

Division of Materials and Manufacturing Science, Graduate School of Engineering, Osaka University, 2-1 Yamadaoka, Suita, Osaka 565-0871, Japan

ARTICLE INFO

Keywords:
Photoreactive MPC polymer
Stripe-micropatterned titanium substrate
Osteoblast orientation
Apatite/collagen orientation
Bone regeneration

ABSTRACT

Titanium (Ti) implants are well known for their mechanical reliability and chemical stability, crucial for successful bone regeneration. Various shape control and surface modification techniques to enhance biological activity have been developed. Despite the crucial importance of the collagen/apatite bone microstructure for mechanical function, antimicrobial properties, and biocompatibility, precise and versatile pattern control for regenerating the microstructure remains challenging. Here, we developed a novel osteogenic tailoring stripe-micropatterned MPC-Ti substrate that induces genetic-level control of oriented bone matrix organization. This biomaterial was created by micropatterning 2-methacryloyloxyethyl phosphorylcholine (MPC) polymer onto a titanium (Ti) surface through a selective photoreaction. The stripe-micropatterned MPC-Ti substrate establishes a distinct interface for cell adhesion, robustly inducing osteoblast cytoskeleton alignment through actin cytoskeletal alignment, and facilitating the formation of a bone-mimicking-oriented collagen/apatite tissue. Moreover, our study revealed that this bone alignment process is promoted through the activation of the Wnt/β-catenin signaling pathway, which is triggered by nuclear deformation induced by strong cellular alignment guidance. This innovative material is essential for personalized next-generation medical devices, offering high customizability and active restoration of the bone microstructure.

Statement of Significance: This study demonstrates a novel osteogenic tailoring stripe-micropatterned MPC-Ti substrate that induces osteoblast alignment and bone matrix orientation based on genetic mechanism. By employing a light-reactive MPC polymer, we successfully micropatterned the titanium surface, creating a biomaterial that stimulates unidirectional osteoblast alignment and enhances the formation of natural bone-mimetic anisotropic microstructures. The innovative approach of regulating cell adhesion and cytoskeletal alignment activates the Wnt/β-catenin signaling pathway, crucial for both bone differentiation and orientation. This study presents the first biomaterial that artificially induces the construction of mechanically superior anisotropic bone tissue, and it is expected to promote functional bone regeneration by enhancing bone differentiation and orientation—targeting both the quantity and quality of bone tissue.

1. Introduction

Efficient bone regeneration through implantation necessitates the rapid formation of intricate microstructures and a stable bond between the material and bone tissue. Titanium (Ti) implant materials, known for their mechanical reliability, chemical stability, and ability to induce osseointegration, play a vital role in treating bone diseases [1,2], and numerous strategies have been developed to enhance the effectiveness of titanium biomaterials [3,4]. Various surface modification techniques, such as sandblasting, acid etching, anodization, plasma spraying, and laser irradiation, have been developed to generate effective biomaterials [5–7]. These processes modify several material surface characteristics, including shape, roughness, and chemical composition, significantly influencing cell migration, alignment, gene expression, and differentiation—crucial factors for bone regeneration speed, bone compatibility, and material-tissue bond stability [8–11].

Bone tissue, comprising collagen and apatite, exhibits a hierarchical anisotropic structural organization from macro to micro levels [12–14]. In intact bone, apatite crystals align along collagen fibers, resulting in anisotropic mechanical properties of the oriented bone tissue [15,16].

* Corresponding authors at: Division of Materials and Manufacturing Science, Graduate School of Engineering, Osaka University, 2-1 Yamadaoka, Suita, Osaka 565-0871, Japan.

E-mail addresses: matsugaki@mat.eng.osaka-u.ac.jp (A. Matsugaki), nakano@mat.eng.osaka-u.ac.jp (T. Nakano).

https://doi.org/10.1016/j.actbio.2024.12.017
Received 3 September 2024; Received in revised form 21 November 2024; Accepted 5 December 2024
Available online 6 December 2024
1742-7061/© 2024 The Authors. Published by Elsevier Ltd on behalf of Acta Materialia Inc. This is an open access article under the CC BY license (http://creativecommons.org/licenses/by/4.0/).

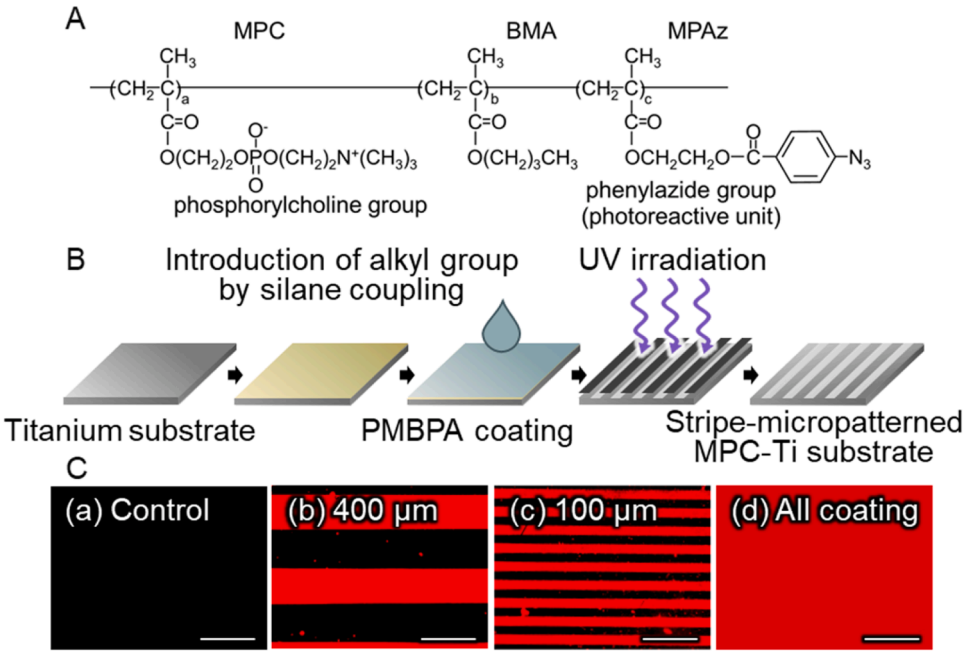

Fig. 1. Fabrication of Stripe-micropatterned MPC-Ti substrates for cell adhesion regulation. (A) Chemical structure of the photoreactive phospholipid polymer poly(MPC-co-BMA-co-MPAz) [PMBPAz]. (B) Schematic illustration of the fabrication method for stripe-micropatterned MPC-Ti substrate. (C) Rhodamine-stained images of stripe-micropatterned MPC-Ti substrates: (a) Complete UV shielding (control), (b) partial shielding 400 μm, (c) 100-μm-wide pattern, and (d) surface covered entirely with MPC polymer without shielding. Scale bar, 500 μm.

This anisotropic microstructure varies according to the anatomical site and is precisely regulated by the surrounding mechanical environment of each bone tissue [17]. Constructing anisotropic structures is the most efficient way to endure anisotropic stress fields acting on bones. Indeed, employing a rat ulnar loading model, we demonstrated that bone adapts its mechanical properties by changing apatite orientation in response to uniaxial strain stimuli [18]. However, organizing the oriented bone matrix during fractured bone recovery requires markedly more time than bone filling [19]. This lack of microstructural restoration is due to the immature state of the filling bone, which cannot adequately sense stress [20,21]. Consequently, achieving complete and natural recovery of bone function after a fracture is complex, and the risk of refracture is high. To overcome this challenge from the perspective of bone tissue engineering, it is essential to develop biomaterials capable of controlling collagen/apatite orientation from the early stages of recovery.

Previous studies showed that a well-ordered array of mesenchymal stem cells (MSCs) and osteoblasts promotes the regeneration of anisotropic bone tissue [22–24]. Specifically, materials with unidirectional patterns have proven beneficial in restoring the anisotropic microstructure of collagen/apatite bone matrix [25–28]. Cell arrangement and movement are induced by adhesion to the scaffold and subsequent realignment of the cell cytoskeleton [21,29,30]. Osteoblasts extending in one direction form aligned collagen fibers and deposit calcified substrates on these fibers [23,31]. A well-constructed, oriented bone matrix shows better resistance to bacterial growth than disordered bone tissue [32]. Therefore, incorporating orientation patterns during bone recovery not only enhances mechanical strength but also prevents postoperative infection. Furthermore, achieving precise and versatile patterning control is essential for establishing freely aimed orientation structures and site-specific customization.

Here, we propose a novel biomaterial—a stripe-micropatterned MPC-Ti substrate—that facilitates the construction of an oriented bone matrix based on genetic-level control by regulating cell adhesion behavior. This approach mimics the natural anisotropic structure of bone, associated with the aligned collagen/apatite microstructures formation which are essential for restoring the mechanical properties of damaged bone. Successful micropatterning of 2-methacryloyloxyethyl phosphorylcholine (MPC) polymer on pure Ti substrates using light-reactive MPC polymer was achieved. Owing to its high hydrophilicity and nontoxic nature, the MPC polymer provides precise control over cell adhesion. This patterned device robustly aligned with the cytoskeleton of osteoblasts by providing a distinct interface for regulating cell adhesion. Inducing the arrangement and extension of osteoblasts enhanced the collagen/apatite orientation structure along the micropattern. Moreover, it triggered gene activation, promoting bone differentiation through the activation of the Wnt/β-catenin signaling pathway. Our approach using MPC-Ti substrates highlights a strategy to promote the construction of mechanically superior anisotropic bone tissue by artificially controlling osteoblast adhesion and the cytoskeleton. This novel patterned biomaterial enables the restoration of bone microstructure and exhibits high customizability, making it indispensable for next-generation personalized medical devices.

2. Materials and methods

2.1. Materials

The MPC polymer was acquired from NOF Co. (Tokyo, Japan) and used without further purification. Reagent-grade thionyl chloride and 4-azidobenzoic acid were purchased from Tokyo Chemical Industry Co., Ltd. (Tokyo, Japan). Triethylamine (TEA), 2-hydroxyethyl methacrylate (HEMA), and n-butyl methacrylate (BMA) were purchased from Kanto Chemical Co., Inc. (Tokyo, Japan), and n-octadecyltrichlorosilane (ODS) was purchased from Sigma-Aldrich (St. Louis, MO, USA). HEMA and TEA were refined through distillation, and the fractions were collected at their boiling points (74 °C/0.6 kPa and 87 °C, respectively). All other reagents and solvents were commercially available.

2.2. Synthesis of photoreactive mpc polymer

MPAz was synthesized using a previously reported method [33,34]. In brief, 4-azidobenzoyl chloride (9.0 g, 0.050 mol) was dissolved in diethyl ether (80 mL) and cooled to −2 °C. A diethyl ether solution (50 mL) containing both HEMA (50 mmol) and TEA (50 mmol) was then

added and stirred for 1 h After the mixture reacted for 20 h, the resulting triethylamine hydrochloride was filtered, and the unreacted fraction was extracted using aqueous HCl (10 mM). The diethyl ether layer was dehydrated using anhydrous magnesium sulfate. Subsequently, magnesium sulfate was removed by filtration, and the solvent was evaporated under reduced pressure. Finally, MPAz was obtained as a light yellow oil, which transformed into a light yellow solid upon storing at −20 °C.

The structure of MPAz was analyzed by ^{1}H nuclear magnetic resonance (NMR) spectroscopy in $CDCl_3$ and Fourier-transform infrared spectroscopy (FT–IR; FT–IR-6300, JASCO, Tokyo, Japan). The NMR results were as follows (ppm): 1.95 (s, 3H, α-CH_3), 4.47−4.53 (q, 2H, $-CH_2CH_2$), 4.55−4.58 (q, 2H, $-CH_2CH_2$), 5.59 (s, 1H, $=CH_2$), 6.14 (s, 1H, $=CH_2$), 7.06−7.09 (d, 2H, benzyl), 8.02−8.05 (d, 2H, benzyl). The IR results were as follows (cm^{-1}): 3022 (p-Ar), 2121 (C − N_3), 1718 (C = O), 1604 (C = C).

Poly(MPC-co-BMA-co-MPAz) [PMBPAz] was synthesized employing a conventional radical polymerization method in ethanol, using 2,2-azobisisobutyronitrile (AIBN) as an initiator at 60 °C (Fig. 1A). The concentrations of monomers and AIBN were 0.5 mol/L and 2.5 mmol/L, respectively. Following a 15-h reaction, the reaction mixture was poured into an excess of diethyl ether:chloroform (80:20 v/v) to precipitate the polymer. The precipitated polymer was then filtered and redissolved in water for purification via dialysis against water in the dark, using a dialysis membrane (molecular weight cutoff of 3000). Subsequently, the aqueous polymer solution was freeze-dried (yield 58 %). The chemical structure of PMBPAz was confirmed using ^{1}H NMR (Fig. S1). The molecular weights of the polymer were evaluated by gel permeation chromatography in a water/methanol mixture (30:70 v/v), and their retention times were compared with those of poly(ethylene glycol) standard samples (Tosoh Co., Tokyo, Japan).

The compositions of each monomer unit in the polymer, including MPC, BMA, and MPAz, were 70 %, 21 %, and 9 mol%, respectively. The weight-averaged molecular weight of the PMBPAz was 7.4×10^4, and its molecular weight distribution was 3.1.

2.3. Patterning and visualization of mpc polymer on Ti substrates

MPC polymer patterns were generated on Ti surfaces using PMBPAz (Fig. 1B). A square Ti substrate measuring 10 × 10 mm was obtained from a pure Ti plate with a thickness of 0.5 mm. Its surfaces were polished until a mirror finish was achieved and cleaned by ultrasonic treatment with acetone and ethanol for 15 min each. After drying, alkyl groups were introduced into the substrates through silane coupling, as detailed in previous studies [35]. The silanization process was performed by dissolving 10 mM ODS in anhydrous toluene and immersing the Ti substrate in the ODS solution at 80 °C for 24 h The Ti substrate was washed thrice with toluene and dried at 23 °C under vacuum. Silanized Ti was then coated with PMBPAz [34]. A PMBPAz solution (0.5 wt.% in ethanol) was applied to Ti substrates, followed by drying and immobilization through UV irradiation. During UV irradiation, a light-shielding mask was used to create three types of substrates with varying cell adhesion zone widths: no pattern, 100 μm, and 400 μm. Subsequently, the samples were subjected to ultrasonic treatment with ethanol for 5 min and then dried.

The MPC polymer patterns were visualized through rhodamine staining (Fig. 1C). The samples were immersed in a 200 ppm Rhodamine 6 G solution (Sigma-Aldrich) for 30 s and rinsed twice with sterile water. The stained images were observed under a fluorescence microscope (BZ-X710; Keyence, Osaka, Japan) at an excitation wavelength of 546 nm.

2.4. Isolation and culture of osteoblasts

To isolate primary osteoblasts, a sequential enzymatic process was employed using calvariae obtained from 3-day-old C57BL/6 mice. The calvariae were carefully extracted and immediately immersed in ice-cold α-MEM (Invitrogen, Thermo Fisher Scientific, Carlsbad, CA, USA). Meticulous removal of the fibrous tissues surrounding the bone was followed by fine cutting of the calvariae, which were thoroughly washed with Hanks' balanced salt solution (Gibco, Thermo Fisher Scientific, Grand Island, NY, USA) to ensure cleanliness. The extracted calvariae were then subjected to five rounds of treatment with a combination of collagenase and trypsin (collagenase: Wako, Osaka, Japan; trypsin: Nacalai Tesque, Kyoto, Japan) at 37 °C for 15 min per round. The supernatants obtained from the initial two treatments were discarded, while those from the third, fourth, and fifth treatments were collected in α-MEM. Subsequently, the collected samples were filtered using a 100-μm-mesh strainer (BD Biosciences, San Jose, CA, USA) and then centrifuged to remove the supernatant. To facilitate cell culture, the resulting cells were resuspended in α-MEM supplemented with 10 % fetal bovine serum (FBS; Gibco), 1 % penicillin, and streptomycin (Invitrogen). Animal experimentation guidelines were strictly followed, and all procedures received approval from the Osaka University Committee for Animal Experimentation (Approval No 2020–1–0). The isolated osteoblasts were seeded onto Ti substrates with a MPC polymer pattern at a density of 8000 cells/cm^2, and incubated at 37 °C in an environment with 5 % CO_2.

2.5. Immunofluorescence staining

Osteoblasts on stripe-micropatterned MPC-Ti substrates were fixed with 4 % formaldehyde in phosphate-buffered saline (PBS) at 23 °C for 20 min, followed by rinsing with PBST (PBS-0.05 % Triton X-100) to remove residual formaldehyde. Non-specific binding sites were blocked by incubating the cells in a PBST solution containing 1 % normal goat serum (Invitrogen) at 23 °C for 30 min. For vinculin immunostaining, the cells were incubated overnight at 4 °C with mouse anti-vinculin monoclonal antibodies (Sigma-Aldrich). After washing with PBS, the cells were treated with secondary antibodies (Alexa Fluor 546-conjugated anti-mouse IgG, Invitrogen) along with DAPI (Invitrogen) and further incubated at 23 °C for 2 h To visualize F-actin, cells were treated with Alexa Fluor 488-conjugated phalloidin (Invitrogen), rinsed with PBST, and mounted using Prolong Diamond Antifade Reagent (Invitrogen) before observing under a fluorescence microscope (BZ-X710; Keyence). Collagen I was stained and observed using the same method, employing primary (anti-collagen I rabbit polyclonal antibody; Sigma-Aldrich) and secondary (Alexa Fluor 546-conjugated anti-rabbit IgG; Invitrogen) antibodies. Antibodies used in this study are listed in Supplementary Table 1.

2.6. Oriented collagen gel fabrication

Rat-tail type I collagen (BD Biosciences) was prepared at a concentration of 10 mg/mL in 0.02 N acetic acid. A hydrodynamic extrusion method was used to produce oriented collage substrates [36], employing a syringe needle for string-type and flat needle for sheet-type orientations. Deposition into 10× PBS, was controlled by a three-axis robotic arm (SM300–3A; Musashi Engineering, Tokyo, Japan), regulating the direction of the collagen molecular fibrils. Control substrates without preferential orientation were fabricated by depositing a collagen type I solution onto a flat surface, followed by gelation in PBS and dehydration. The substrates were immersed in sterile PBS for 6 h before cell seeding to induce sufficient swelling.

2.7. Cytoskeletal protein disruption

Depolymerization of actin filaments and microtubules was induced by treating them with cytochalasin D (Sigma-Aldrich) and colchicine (Sigma-Aldrich), respectively, for 1 h, followed by two washes with fresh medium. The treatment was started after 7 days of cultivation and repeated every 3 days. The reagents were dissolved in dimethyl sulfoxide (Sigma-Aldrich) or distilled water and added to vehicle groups.

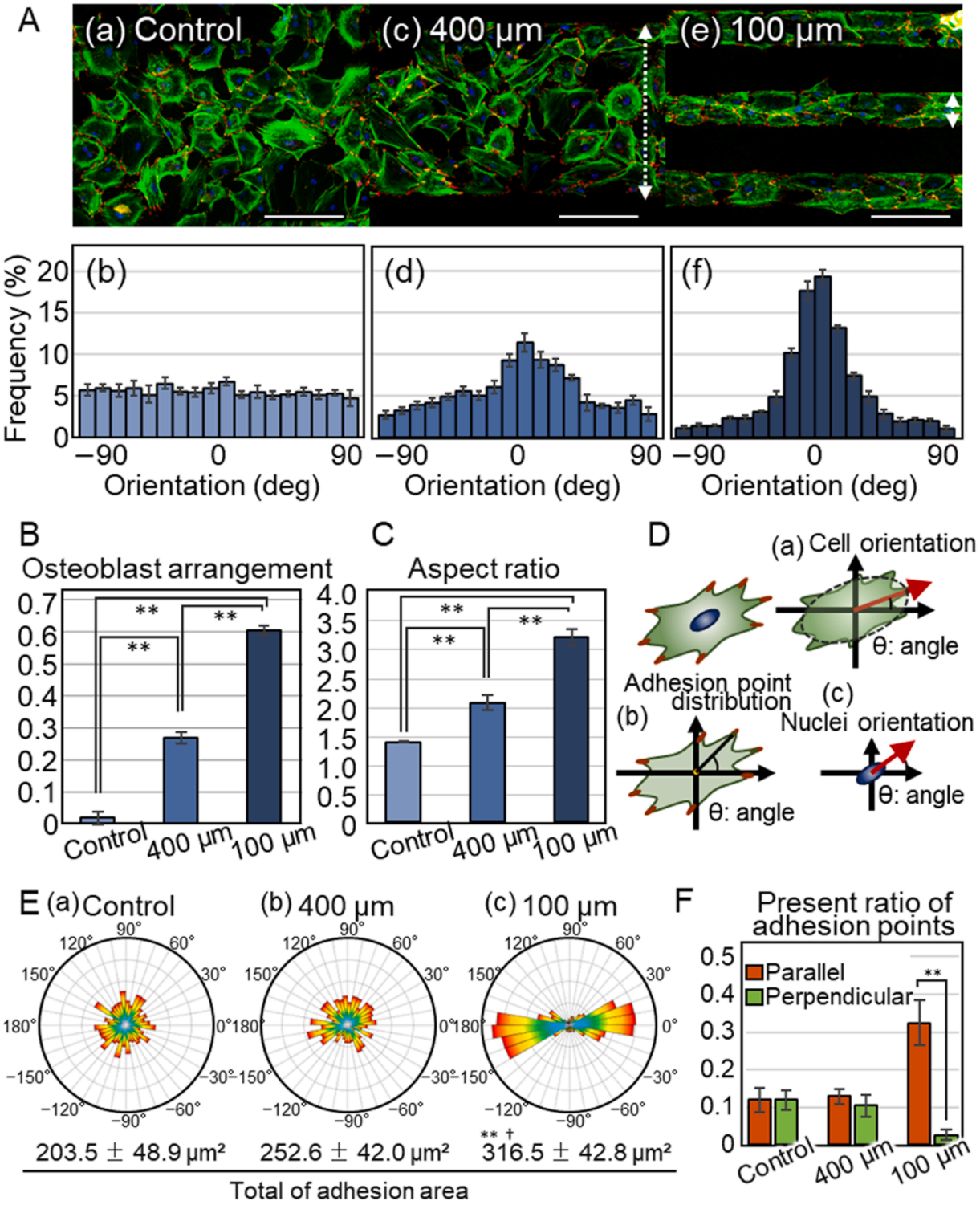

Fig. 2. Controlling osteoblast arrangement through a novel patterned substrate with regulated cell adhesion. (A) Immunostaining images and orientation distribution of osteoblasts on MPC polymer patterns at each width: (a) and (b), control; (c) and (d), 400 μm; and (e) and (f), 100 μm. Scale bar, 200 μm. (B) Quantitative analysis of osteoblast orientation. (C) Quantitative analysis of aspect ratio on patterned substrates. (D) Schematic representation of the quantification of cellular orientation, nuclear orientation, and adhesive point distribution in osteoblasts. (E) Distribution of adhesive points in osteoblasts on patterned substrates. The angle distribution of adhesion spots is shown at 10° intervals, with the total adhesion area displayed below. ** $p < 0.01$ vs. control, † $p < 0.05$ vs. 400 μm. (F) Presence ratio of adhesion zones in the parallel and perpendicular directions of the micropatterns. The ±30° range from 0° or 180° were defined as parallel, and the ±30° range from −90° or 90° were defined as perpendicular. $n = 5$; ** $p < 0.01$.

2.8. Alizarin red s staining

Calcium deposition was visualized using Alizarin Red S staining. Cells were washed with PBS, fixed in 10 % formaldehyde for 20 min, washed with distilled water, and then stained with 1 % Alizarin Red S solution (Wako, Osaka, Japan) for 30 min. Excess dye was removed by washing thrice with distilled water.

2.9. Cell orientation analysis

To quantitatively evaluate cell orientation relative to the unidirectional adhesion zones on the Ti substrate, fluorescent cell images were acquired using a fluorescence microscope (BZ-X710; Keyence). Cell orientation was quantified using the Cell Profiler software (Broad Institute, Cambridge, MA, USA). The degree of cell organization, denoted as R, was determined using the following previously established equation [37]:

$$R = 2\left(\langle \cos^2\theta \rangle - \frac{1}{2}\right) \quad (1)$$

$$\langle \cos^2\theta \rangle = \left(\sum_{1}^{n} \cos^2\theta\right) \Big/ n \quad (2)$$

2.10. Gene expression analysis

Osteoblast RNA was extracted using the NucleoSpin RNA Plus XS (Macherey-Nagel GmbH & Co. KG, Düren, Germany) according to the manufacturer's protocol. Briefly, cells were lysed and the resulting lysate was filtered to remove impurities. The RNA was subsequently bound to a column, washed with ethanol-containing wash buffer, and finally eluted and collected in RNase-free water. Isolated RNA was reverse transcribed using the Step One RT–PCR system (Applied Biosystems, Foster City, CA, USA) in a total volume of 20 μL. Relative gene expression changes were calculated using the ΔΔCt method employing the Taqman® Gene Expression Assay primer and probes. Primers used are listed in Supplementary Table 2.

2.11. Luciferase assay

Osteoblasts were transfected with the β-catenin-responsive firefly luciferase reporter plasmids TopFlash (Addgene, Cambridge, MA, USA). To control the transfection efficiency, FopFlash plasmids (Addgene) were also transfected. After culturing for 48 h, the cells were lysed and assayed for firefly and Renilla luciferase activities, according to the manufacturer's instructions (Promega, Madison, WI, USA). Firefly luciferase activity was normalized to the transfection efficiency using Renilla luciferase activity.

2.12. Raman microscopy measurements and data processing

To investigate collagen orientation in the bone matrix formed by osteoblasts, Raman spectra were obtained using a laser Raman spectrophotometer (NRS-5100, Nihon Bunko, Tokyo, Japan) across a wide spectral range of approximately 300–3900 cm^{-1}. Before the measurement, the spectrophotometer was calibrated using an Si reference sample, and the samples were oriented to align with the MPC polymer pattern at 0° polarization. Raman spectra were acquired at 20× magnification, with the sample rotated 30° in each direction. Subsequently, the intensities of specific chemical bonds, namely C = O (carbonyl group) at 1664 cm^{-1} and C–H at 1435 cm^{-1}, were analyzed. We observed that the carbonyl group of the collagen molecule (C = O) bonded perpendicularly to the peptide chain.

Amide I band intensity is higher when the polarization direction of the laser Raman microscope is perpendicular to the running direction of the collagen fibers [38,39]. Conversely, the C–H bond intensity in collagen molecules remains relatively constant for any polarization direction [38,40]. Exploiting this principle, the degree of collagen molecule alignment was quantitatively evaluated by normalizing C = O bond intensity to C–H bond intensity. In other words, a higher ratio of C = O to C–H indicates a higher degree of alignment, reflecting a perpendicular relationship with collagen molecules.

2.13. Scanning electron microscopy (SEM)

The collagen-calcified matrix formed by osteoblasts was observed using field-emission scanning electron microscopy (FE–SEM; JIB-4610F, JEOL, Japan). Dehydrated samples were prepared in the same manner as that used for Raman spectroscopy, and observed after gold–palladium coating.

2.14. Microbeam X-ray diffraction analysis

To assess the degree of preferential orientation of the apatite *c*-axis in the bone matrix, micro X-ray diffraction (μ-XRD; BQ, Rigaku, Japan) was conducted, based on previously described conditions [26]. The incident beam was focused using a metal collimator, resulting in a beam spot with a diameter of 300 μm, which enabled data collection across a wide range of averaged information. Scattered diffraction patterns were measured for 10,000 s to secure appropriate diffraction intensities. The diffraction peaks (002) and (211) were selected as representatives of the apatite crystal structure. The intensity ratio of these two peaks, appearing at Bragg angles of approximately 11.8° and 14.5°, respectively, was measured to determine the preferential orientation of the apatite *c*-axis [26]. The (002) peak corresponds to the c-axis direction of the hexagonal apatite crystal structure, and its intensity is dependent on the amount of apatite crystals aligned along the c-axis. In contrast, the (211) peak arises from planes that are distributed in various directions, making its intensity independent of the c-axis orientation. By calculating the ratio of (002) to (211), the normalized c-axis orientation of the apatite crystals is indicated. The intensity ratio of randomly oriented apatite (specifically hydroxyapatite) powder (NIST #2910) on the XRD system was 0.12, which served as a benchmark for evaluating the preferential orientation of the apatite *c*-axis in bone matrix samples. The intensity ratios obtained from five different points were collected and averaged for each sample.

2.15. Statistical analysis

All quantitative results are expressed as the mean ± standard error of the mean. Group differences are indicated using the following symbols: * for $p < 0.05$, ** for $p < 0.01$, and NS for not significant. The study was performed with $n = 5$ or $n = 6$. The significance of differences in Raman spectroscopy results between the two samples was assessed using a *t*-test. Other results were compared using one-way analysis of variance (ANOVA), followed by Tukey's test.

3. Results

3.1. Controlling osteoblast arrangement through a novel patterned substrate with regulated cell adhesion

The stripe-micropatterned MPC-Ti substrates were created through UV irradiation using masks of varying widths (Fig. 1A and B). Precise control of MPC polymer patterning was confirmed by Rhodamine staining (Fig. 1C). To manipulate cell morphology, adhesion-modulating patterns of varying widths (50 μm, 100 μm, 200 μm, and 400 μm) were applied to Ti using a photoreactive MPC polymer. Osteoblast behavior on micropatterns of varying widths was visualized via immunostaining 3 days after seeding (Fig. 2A). On each substrate, osteoblasts selectively adhered to uncoated Ti surface areas, avoiding those coated with MPC polymer, despite the absence of cytotoxic effects. The cell morphology

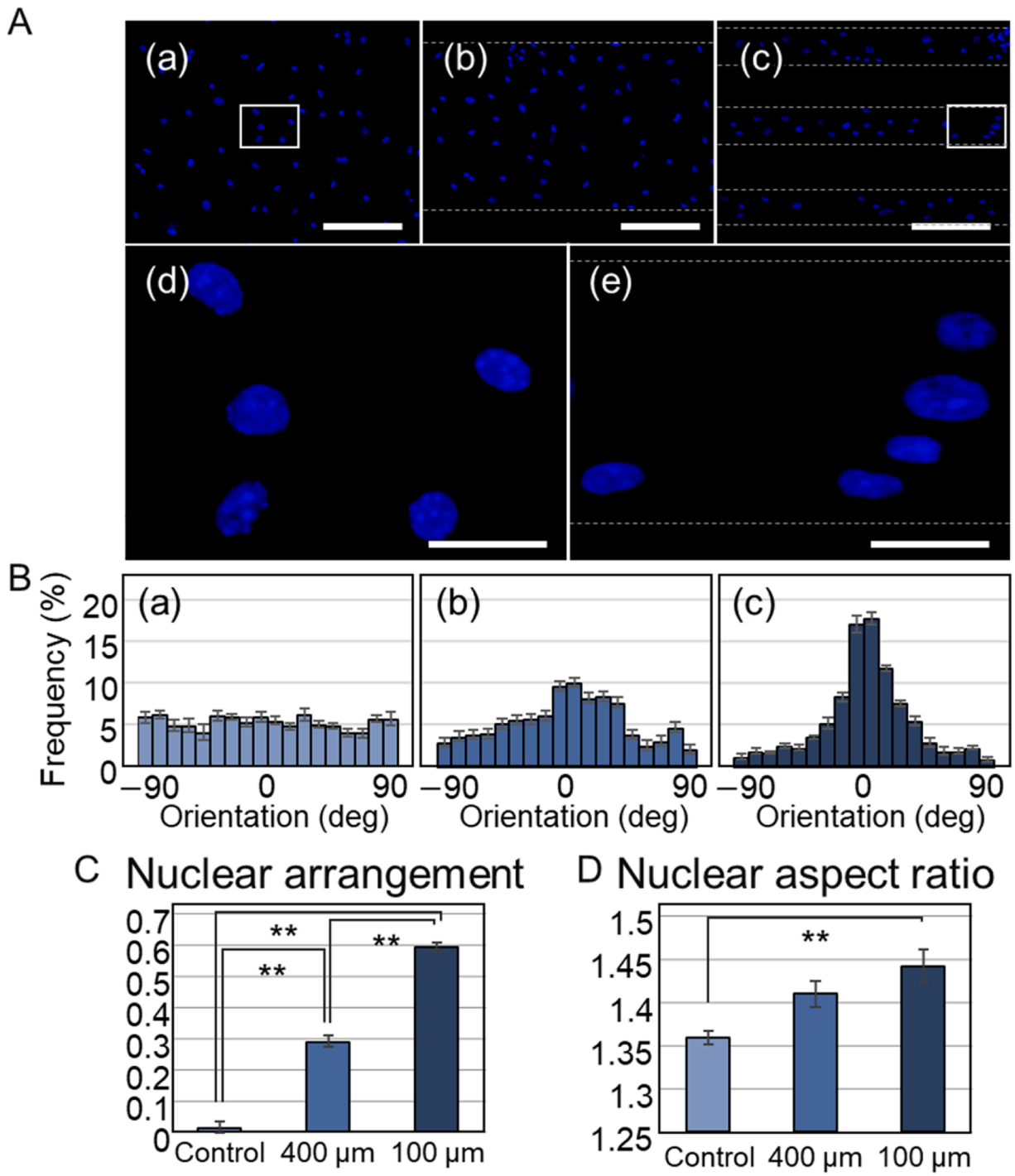

Fig. 3. Nuclear arrangement and deformation induced by actin cytoskeletal alignment in highly aligned osteoblasts. (A) Immunostaining images showing osteoblast nuclei on patterned substrate. (a) Control, (b) 400 μm, (c) 100 μm. Scale bar, 200 μm. (d) and (e) magnified images of the white square regions shown in (a) and (c), respectively. Dashed lines indicate the positions of the MPC polymer patterns. Scale bar, 100 μm. (B) Orientation distribution of nuclei. (C) and (D) Quantitative analysis of (C) nuclear arrangement and (D) nuclear aspect ratio on patterned substrates. $n = 5$; ** $p < 0.01$.

depended on adhesion zone width and showed isotropic spreading on non-adhesion-restricted substrates without MPC polymer patterns. However, on patterned substrates, osteoblasts exhibited a loose arrangement along the pattern direction for 400 μm width and strongly controlled arrangement for 100 μm width. The histograms of cell orientation direction and frequency specifically focused on substrates with 100 μm wide patterns, contrasting with the flat distribution in the control (Fig. 2Ab,d,f). The quantitative arrangement of osteoblasts increased significantly in the order of control without pattern, 400 μm width, and 100 μm width (Fig. 2B). Osteoblasts on substrates with 100 μm wide patterns were the most elongated and arranged along the long axis of the pattern (Fig. 2C). Osteoblasts on 200 μm pattern showed a relatively weak cell alignment comparable to the 400 μm pattern. In the case of the 50 μm pattern, while the cells were arranged in a single line, they failed to form a proper cell network (Fig. S2). To elucidate the effect of the MPC polymer pattern on cell adhesion distribution, the percentage of cell adhesion spots was analyzed at different angles relative to the MPC polymer pattern direction. Osteoblasts on the 100 μm substrate

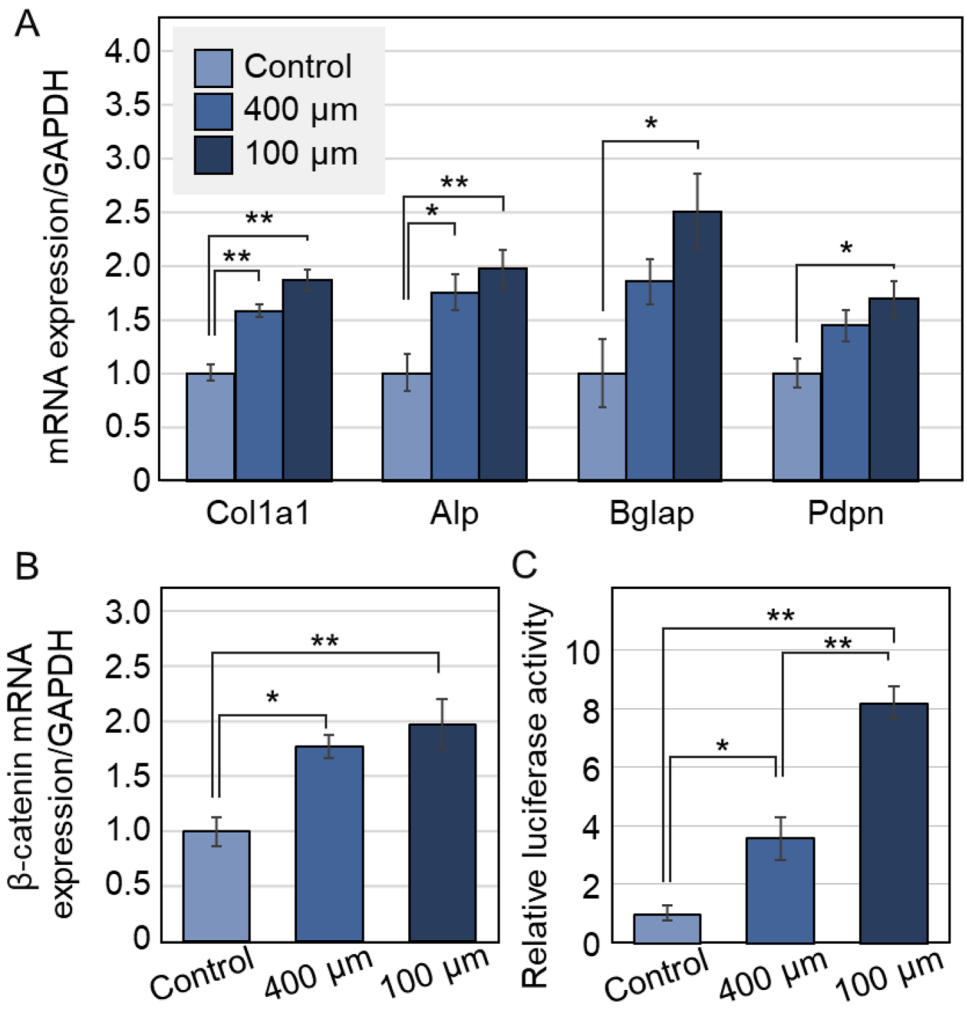

Fig. 4. Enhanced bone differentiation in highly oriented osteoblasts by restricting adhesion zones. (A) Expression analysis of osteogenic differentiation-related genes in osteoblasts on patterned substrates with varying widths. The expression levels are presented as fold-increase over the gene expression levels on the control substrate. (B) Expression analysis of β-catenin. (C) Activation of canonical Wnt/β-catenin signaling measured using a luciferase reporter assay. The obtained luciferase activity is presented as fold-increase over the luciferase activity of osteoblasts cultured on the control substrate. $n = 6$; * $p < 0.05$, ** $p < 0.01$.

showed a significantly higher number of adhesion spots at approximately 0° and 180°, indicating strong preferential adhesion in one direction (Fig. 2D–F). In contrast, those on the 400 μm substrate showed a less pronounced preferential distribution. To demonstrate the differences in adhesion strength, the adhesion distribution area was quantitatively evaluated. The largest adhesion area was observed on the 100 μm substrate, where unidirectional cell extension maximized and enhanced adhesion.

3.2. Enhanced bone differentiation in highly oriented osteoblasts by restricting adhesion zones

Nuclear morphology was analyzed to assess nuclear deformation caused by changes in cell body. In the control, the direction of the nuclei, similar to that of cell bodies, was random, whereas on the stripe-micropatterned substrates, they were preferentially aligned, depending on the width of the micropattern (Fig. 3A–C). Moreover, the nuclear aspect ratio significantly increased on the 100 μm substrate (Fig. 3D). The expression of bone differentiation-related genes in osteoblasts cultured for 4 weeks varied with adhesive zone width (Fig. 4A). The expression of *Col1a1* and *Alp*, expressed in early stages of differentiation, increased in osteoblasts cultured on 400 and 100 μm substrates compared with that in the control. Furthermore, osteoblast differentiation-related genes *Bglap* and *Pdpn*, expressed in late-stage osteoblasts and early-stage osteocytes, respectively, significantly increased in osteoblasts cultured on the narrowest-width substrate. Furthermore, as the cytoskeleton aligned strongly, *β-catenin* expression in osteoblasts increased (Fig. 4B), accompanied by an upregulation of the Wnt/β-catenin signaling reporter (Fig. 4C).

3.3. Regulation of collagen and apatite crystal orientation in bone matrix using micro-patterned substrate

On the micropatterned Ti surface, an anisotropic bone matrix was formed by differentiated osteoblasts after 4 weeks of seeding. Immunostaining revealed the sparse formation of collagen I on the unpatterned substrate (Fig. 5Aa). In contrast, the 100 μm pattern exhibited collagen bundles aligned in the direction of the pattern. Raman microscopic analysis of the bone matrix region yielded spectra of several bonds characteristic of collagen (Fig. 5Ab and c). Collagen orientation was assessed by analyzing the intensity ratio of the C−H (near 1450 nm^{-1}) and C = O (near 1680 nm^{-1}) peaks at 30° intervals from 0° to 360° relative to the pattern direction (Fig. 5B–D). The control was isotropic, showing the same values for all directions. However, the 100 μm pattern substrate showed higher C = O bond ratios in the direction perpendicular to the pattern (90° and 270°), indicating consistent collagen alignment with the MPC polymer pattern (0° and 180°). The quantitative comparison between the parallel and perpendicular

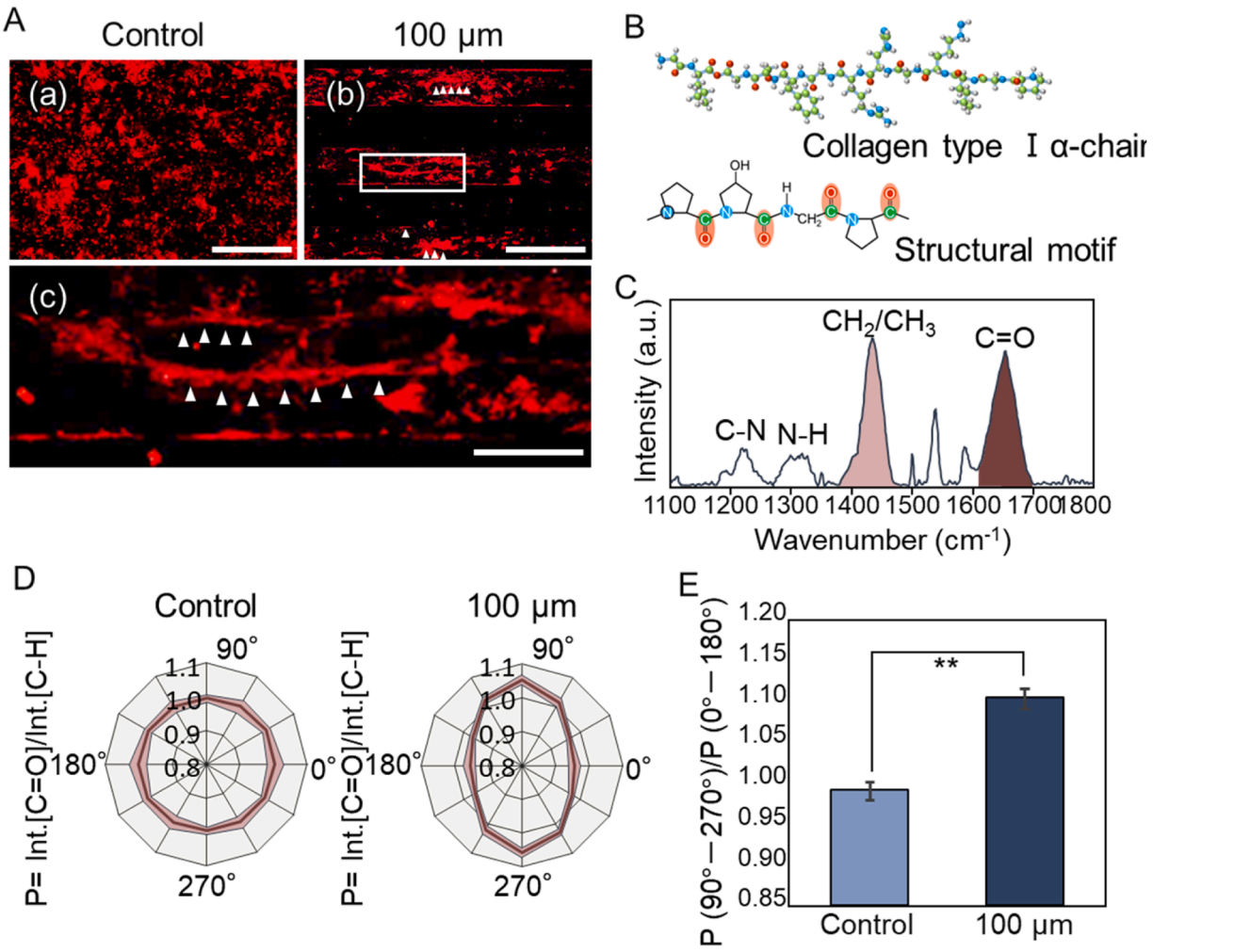

Fig. 5. Highly aligned collagen fibers produced by oriented osteoblasts on micro-patterned substrate. (A) Immunostaining image of type I collagen produced after a 4-week culture of osteoblasts on a patterned substrate: (a) Control, (b) 100 μm. Scale bar, 200 μm. (c) magnified image of the white square region shown in (b). Scale bar, 50 μm. White arrows heads indicate the location of the collagen fibers. (B) Schematic illustration of collagen type I α-chain and its structural motif. (C) Raman spectrum of a representative secretion matrix taken at 0° to the substrate pattern, with intensities normalized to the Raman band at approximately 1435 cm^{-1} (C−H vibration). (D) Fitted elliptical distribution of normalized Raman intensity ratio (C = O/C−H) for a total rotation of 360° (E) Quantitative comparison between the parallel and perpendicular directions for the intensity ratios of the bonding peaks. The normalized Raman intensity ratio (C = O/C−H) was highest when oriented perpendicular to the collagen long chain, aligning with the orientation of C = O bonds. $n = 5$; ** $p < 0.01$.

directions for the intensity ratios of the bonding peaks revealed an anisotropic organization of collagen fibers on the 100 μm pattern substrate compared with that on the control (Fig. 5E).

Osteoblasts cultured for 6 weeks on the Ti substrate formed a calcified bone matrix complexed with collagen fibers. In the control group, membrane-like or weakly fibrotic collagen was formed, and a calcified substrate was developed on these (Fig. 6A). In contrast, when osteoblasts were arranged in a 100 μm adhesion pattern, collagen bundles formed along the pattern, leading to the formation of bone matrix on the oriented collagen. The calcified matrix on each substrate showed an XRD pattern typical of apatite crystals, with sharp peaks corresponding to the (002) and (211) planes (Fig. 6B–D). The (002) plane corresponds to the direction of the apatite *c*-axis, whereas the (211) plane is an orientation-independent crystal plane of apatite. The (002)/(211) intensity ratio, indicative of the apatite crystal orientation, was significantly higher for substrates with a 100 μm pattern. These findings suggest that collagen aligned along the unidirectional cytoskeleton of osteoblasts, with the *c*-axis of apatite crystals epitaxially oriented in that direction.

3.4. Effect of cytoskeletal disruption on the construction of oriented bone matrix

The construction of an oriented bone matrix and associated changes in gene expression, based on adhesion and skeletal regulation on stripe-micropatterned MPC-Ti substrates, were validated on anisotropic collagen substrates mimicking the biological environment. Immunocytochemical analysis revealed that osteoblasts were firmly arranged unidirectionally, along the direction of the collagen substrate (Fig. S3Aa). To clarify the role of the cytoskeleton in cellular arrangement, actin filaments were artificially disrupted for 1 h using cytochalasin D (Fig. S3Ab). After washing in fresh medium, the cytoskeleton became reorganized, realigning along the orientation of the substrate collagen (Fig. S3Ba,b). Alizarin Red S staining revealed that the amount of calcium deposited by osteoblasts treated with inhibitors remained unaffected by the degree of cytoskeletal disruption, depending on the inhibitor concentration (Fig. S3C). The preferential alignment of apatite crystals, analyzed using the integrated intensity ratio of the (002) and (211) peaks along the substrate collagen orientation, showed a decreasing trend in an inhibitor dose-dependent manner (Fig. 7A). A luciferase reporter construct was used to analyze the activation of Wnt/

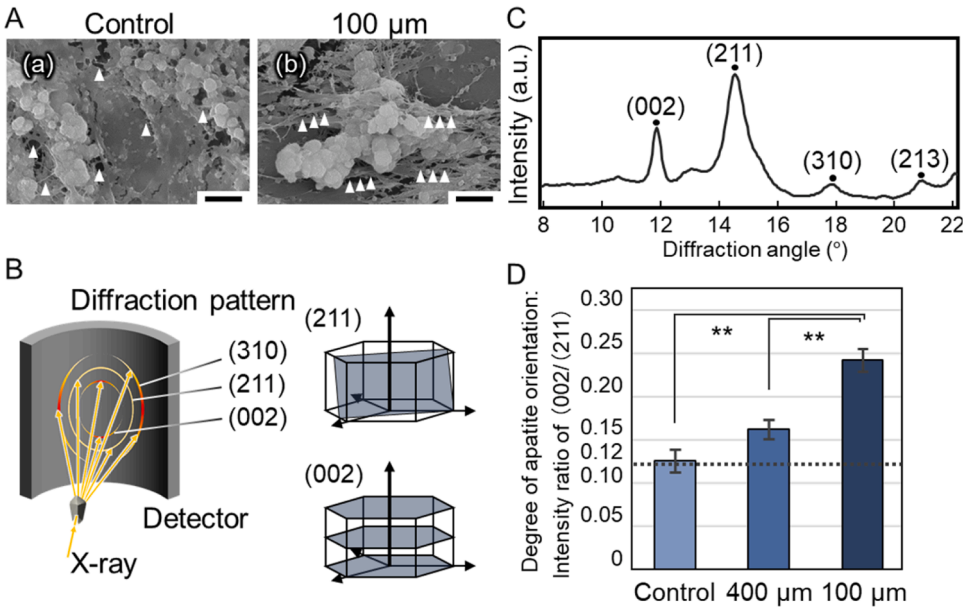

Fig. 6. Regulation of apatite crystal orientation in bone matrix using micro-patterned substrate. (A) SEM images of collagen/apatite composite substrate deposited on a patterned substrate, showing spherical calcifications on fibrous collagen. Scale bar, 5 μm. White arrow heads indicate the location of the collagen fibers. (B) Schematic representation of the quantitative analysis of apatite orientation by X-ray diffraction (XRD). (C) XRD profile of the deposited mineral, indicating typical diffraction peaks of apatite, (002), (211), (310) and (213). (D) Apatite orientation evaluated as the relative ratio of (002)/(211) along the direction of the substrate pattern. $n = 5$; ** $p < 0.01$.

β-catenin signaling in response to dynamic actin cytoskeletal changes. Osteoblasts cultured on the non-oriented control collagen substrates showed basal activation in the absence of additional biochemical cues (Fig. 7B). All luciferase activity values were normalized to this basal activation. Osteoblasts responded to substrate collagen orientation with an approximately 1.5-fold increase in canonical Wnt/β-catenin signaling. Cytochalasin D treatment impaired Wnt/β-catenin activity in arranged cells on oriented collagen substrates, whereas actin disorganization in randomly-oriented osteoblasts cultured on control substrates did not affect Wnt/β-catenin activity. Furthermore, quantitative real-time PCR (qPCR) analysis revealed a decrease to 0.6-fold in *β-catenin* levels in cells arranged along the substrate collagen orientation following cytochalasin D treatment, indicating reduced activation (Fig. 7C). In contrast, the gene expression level of *GSK-3β* slightly increased with actin disruption.

4. Discussion

Bone tissue possesses a precisely oriented microstructure, which provides effective strength in three dimensions to withstand anisotropic external forces. Reconstructing anisotropic bone microstructures by artificially inducing innate mechanisms underlying pattern formation in the bone matrix is essential for effectively restoring damaged bone strength. In this study, we developed an innovative Ti substrate with MPC polymer stripes to artificially promote the construction of an oriented bone matrix based on genetic-level control. Specifically, the actin skeleton and cellular arrangement of osteoblasts were controlled by restricting the cell adhesion region based on hydrophilicity. This regulation not only affected osteoblast arrangement but also promoted bone differentiation, resulting in changes in gene expression and the formation of a unidirectionally oriented collagen/apatite composite bone matrix.

4.1. Stripe-micropatterned MPC-Ti controls osteoblast arrangement via cell adhesion and cytoskeletal reorganization

The MPC polymer patterns were successfully created on Ti substrate surfaces using photoreactive polymerization (Fig. 1B and C). MPC polymer is widely utilized to prevent undesirable biological responses and reactions, owing to its extreme hydrophilicity and electrically neutral nature [41]. In this study, we focused on the on/off spatial switching of cell adhesion via patterned coatings of MPC polymer as a strategy to induce cell alignment on titanium substrates while preserving cell function. The stripe-micropatterned MPC-Ti served as a cue for cell orientation (Fig. 2A). Focusing on the interface between the MPC polymer and osteoblasts, adhesion sites avoided the MPC polymer, preferentially aligning in other directions (Fig. 2E and F). This resulted in actin filaments aligning parallel to the pattern of the osteoblasts near the interface and stress fiber formation along non-adhered edges, consistent with previous studies [42]. Additionally, cells on the 100 μm pattern showed significantly larger adhesion areas. It is well known that the size of focal adhesion sites positively correlates with intracellular tension [43,44]. In other words, by controlling the alignment of cell adhesions, stress fibers align unidirectionally within the cell, with osteoblasts extending in that direction. Cytoskeletal deformation is associated with adhesion sites, and osteoblasts adhere to Ti substrates via integrin α5β1 [45]. Interestingly, in the present study, integrin α5β1 expression showed no significant changes (Fig. S4); however, both the nucleus and cytoskeleton exhibited deformation (Fig. 3A). The regulation of the adhesion sequence induced actin reorganization in one direction, leading to anisotropic nuclear deformation due to actin tension, likely promoting related gene expression (Fig. 4A). In addition, osteoblast orientation was affected by the width of the cell adhesion zone, with loose arrangement along the pattern direction at 400 μm width and strongly controlled arrangement at 100 μm width (Fig. 2A and B). The width of the pattern relative to the cell is crucial for controlling cell behavior [46]. Notably, osteoblasts, approximately 100 μm in size in their natural spread state, showed the strongest arrangement and elongation when in contact with the interface of the 100-μm-wide pattern. In this scenario, almost all osteoblasts should be in contact with the interface, enabling cytoskeleton control through precise on/off adhesion. At 400 μm width, osteoblasts elongated similarly at the interface with the MPC polymer, while those located away from the interface remained unrestricted in their elongation, leading to isotropic or

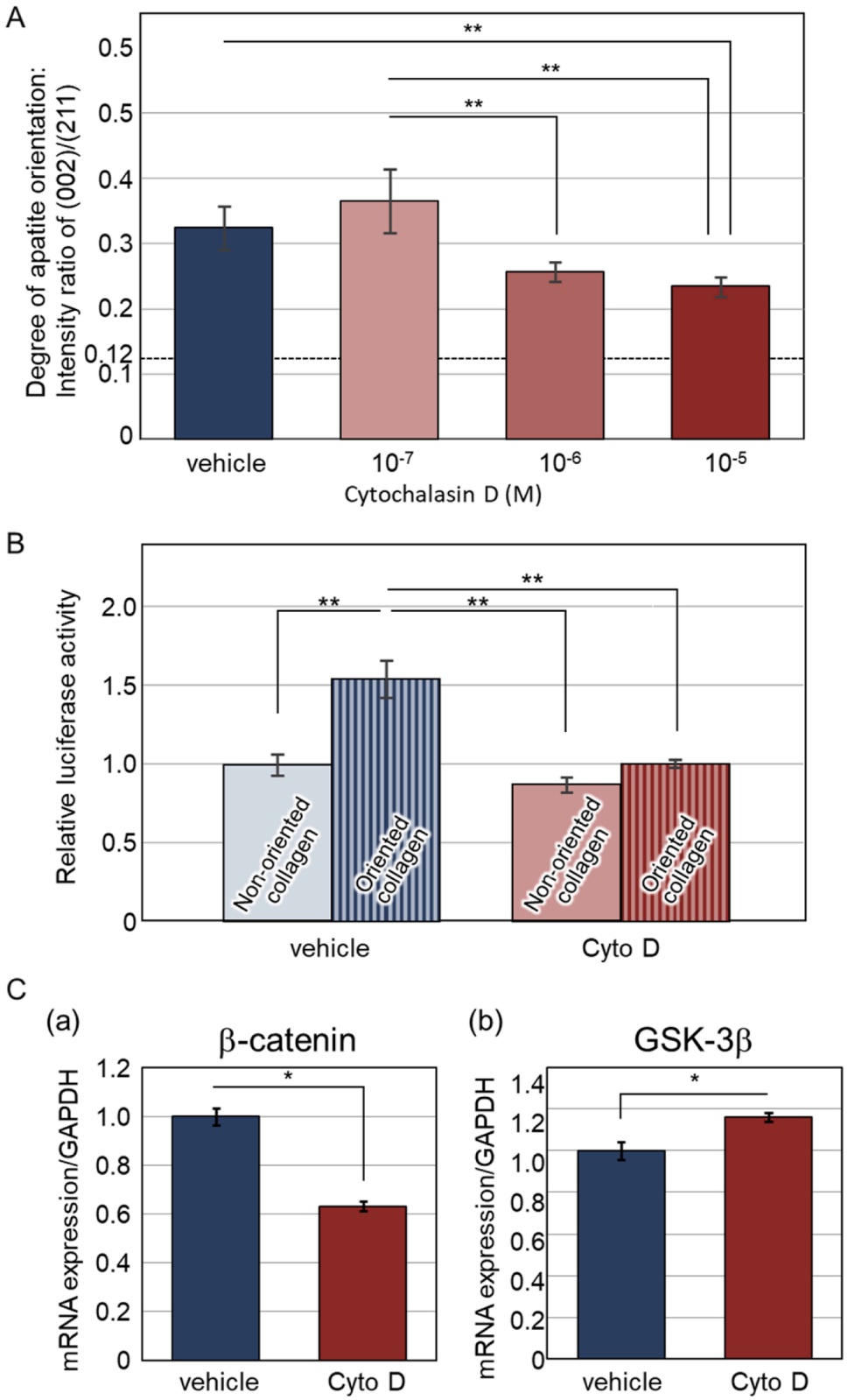

Fig. 7. Effect of cytoskeletal disruption on the construction of oriented bone matrix. (A) Apatite orientation evaluated as the relative ratio of (002)/(211) along the substrate collagen orientation. The preferential orientation of apatite was downregulated by cytochalasin D. (B) Activation of canonical Wnt/β-catenin signaling in osteoblasts measured using luciferase reporter assay. The obtained luciferase activity is presented as fold-increase over the luciferase activity of untreated osteoblasts cultured on non-oriented collagen substrate. (C) Gene expression analysis of cytochalasin d-treated osteoblasts. The obtained expression levels are presented as fold-increase over the gene expression levels of untreated osteoblasts cultured on oriented collagen substrates. $n = 6$; * $p < 0.05$, ** $p < 0.01$.

random elongation, and consequently, weaker cell orientation. A preliminary experiment verified the same for even narrower (50 μm) and intermediate widths (200 μm); however, the 50 μm pattern arranged cells did not provide adequate cell aggregation and could not promote long-term bone formation (Fig. S2A,B). The 200 μm pattern, like the 400 μm pattern, was too wide to effectively control cell adhesion, resulting in insufficient guidance for osteoblast arrangement. Consequently, the optimal adhesion pattern width for controlling cell behavior, strongly dependent on cell size, was 100 μm, proving to be the most effective. The ability to control the cytoskeleton and cell arrangement by selecting the cell adhesion zone width holds promise for similar applications in other cell types, enabling the selection of cell-specific adhesion zone restrictions for the desired anisotropic tissue architecture.

4.2. Controlled unidirectional osteoblast arrangement induces osteogenic differentiation via wnt/β-catenin signaling activation

Regulating gene transcription in response to cell adhesion and cytoskeletal reorganization is crucial for shaping appropriate tissue morphology in both autogenic and regenerative processes. This study shows that controlling cell arrangement by stripe-micropatterned MPC-Ti induces nuclear deformation and even altered bone differentiation-related gene expression. Several studies have reported a correlation between nuclear deformation and gene expression [47,48]. In this study, the transport of β-catenin into the nucleus could be attributed to nuclear elongation in the direction of cell elongation. Cell arrangement-induced enhancement of canonical Wnt signaling has also been reported in studies involving neuronal nanostructures [49]. In our study, modulation of a cell adhesion region induced over 2-fold cellular deformation compared with that of the control, as evident from changes in the cell and nuclear aspect ratios (Fig. 3D), and was sufficient to enhance gene expression [50,51]. The study findings show the activation of Wnt/β-catenin signaling and increased expression of osteogenesis-related genes. Wnt/β-catenin signaling is a widely studied bone differentiation signaling pathway [52–54], where the initiation of Wnt/β-catenin signaling induces the activation and nuclear translocation of β-catenin [55,56], which in turn facilitates the expression of osteogenesis-promoting genes, including *Runx2* [57]. During osteogenesis, osteoblasts express various genes at different stages, including increased expression of *Runx2, ColIa1, Alp*, and *Osx* in the early stages, *Ocn* and *Opn* in the later stages, and *Pdpn* when they become pre-osteocytes [54,58]. In this study, restricting cell adhesion enhanced *ColIa1* and *Alp* expression; furthermore, the 100 μm pattern enhanced *Bglap (Ocn)* and *Pdpn* expression (Fig. 4A). In conclusion, stress fiber regulation and subsequent osteoblast elongation activated the Wnt/β-catenin pathway, inducing bone differentiation. The activation of Wnt signaling in osteoblasts also regulates osteoclast formation and bone resorption through a mechanism that involves the transcriptional repression of the gene encoding receptor activator of NF–κB (Nuclear Factor kappa–light-chain-enhancer of activated B cells) ligand (RANKL or TNFSF11), a key osteoclastogenic cytokine [59,60]. Thus, applying this material to fracture sites may help mitigate excessive osteoclast activity triggered by foreign body recognition, promoting a more balanced bone remodeling process and potentially contributing to the successful healing of fractures. The *in vivo* model will be provided in our future research to make it clear how the above multiple cellular interactions are associated with the developed materials.

4.3. Artificial control of the bone-mimetic oriented collagen/apatite structure as a bone quality index

The bone matrix orientation, including collagen alignment and apatite orientation, plays a crucial role in ensuring proper mechanical bone function. In this study, the formation of hierarchically oriented collagen/apatite matrices was successfully achieved by controlling osteoblast arrangement, the root of bone formation, in a unidirectional adhesion zone pattern. The alignment of collagen fibers matched the cellular arrangement, with long fibers running parallel to the MPC polymer pattern (Fig. 5A). Collagen produced by arranged osteoblasts tends to align parallel to the direction of cell body elongation, influenced by the tension of elongated actin fibers [31]. The inherent three-dimensional orientation of C = O bonds in collagen was analyzed using Raman spectroscopy, albeit within the confines of a two-dimensional plane along the Ti surface, covering a range from 0° to 360° (Fig. 5C and D). Nevertheless, collagen controlled by the pattern was uniaxially oriented and should exhibit unidirectional orientation because the distribution of C = O bonds is similar to that of tendon collagen, which exhibits strong unidirectional collagen orientation [40]. The *c*-axis of the apatite crystals grew in the same direction as the pattern-controlled collagen orientation (Fig. 6C and D). Importantly, the *c*-axis direction of the apatite clearly coincided with the pattern direction, indicating that control of the cytoskeleton through patterning at the substrate surface can determine the crystallographic orientation of the bone matrix. This orientation is crucial for the material integrity of the bone, as apatite crystals exhibit greater mechanical strength in the *c*-axis direction than in other directions [13]. To optimize functionality in an anisotropic mechanical environment, the bone material should exhibit anisotropy rather than isotropy. In fact, it has been demonstrated that bone exhibits distinct orientation patterns at different sites, with the *c*-axis of apatite aligning in the direction of the principal stresses at that site [16]. However, notably, the autonomous recovery of apatite crystalline orientation is a time-consuming process [19]. During bone regeneration, the initial filling is followed by a delayed build-up of an optimal collagen/apatite orientation pattern based on osteocyte stress sensitivity [21,61]. Therefore, biomaterials supporting the construction of orientation are essential for the rapid restoration of bone integrity. A series of intervertebral devices that specifically promote cellular-level bone orientation, including osteoblast arrangements, has recently been developed [62,63]. These devices acquired significant mechanical stability through oriented bone regeneration, similar to the surrounding pre-existing bone. In essence, the apatite crystal orientation achieved through adhesion-controlled patterning *in vitro*, as shown in this study, is expected to be effective *in vivo*.

4.4. Osteoblast cytoskeletal design plays a crucial role in osteogenic tailoring in association with oriented bone matrix organization

This study elucidated that the activation of Wnt/β-catenin signaling through stripe-micropatterned MPC-Ti substrates is a crucial biological mechanism for bone matrix arrangement. The association between bone matrix arrangement and Wnt/β-catenin signaling was investigated on an oriented collagen substrate mimicking the natural bone environment. A previous study showed that osteoblasts arrange along their orientation on collagen substrates [23]. Osteoblasts aligned on the collagen substrate formed oriented apatite matrix and activated Wnt/β-catenin signaling, similar to those on the MPC-Ti substrate (Fig. 7). This suggests that cytoskeletal arrangement is a key regulator of bone anisotropic construction in natural bone formation. The cytoskeleton comprises actin fibers, microtubules, and intermediate filaments. Actin fibers, tethered to intercellular and cell-substrate adhesion apparatuses, form a network throughout the cell [64], playing essential roles in controlling cell morphology, including orientation, by sensing the extracellular environment, such as the surface structure and chemical properties of the substrate [65,66]. To elucidate the role of cytoskeletal alignment in generating highly oriented substrates and activating gene expression, we disrupted the cytoskeleton using the widely accepted actin polymerization inhibitor cytochalasin D [67,68]. This inhibitor treatment resulted in the loss of actin filament polymerization, cytoskeletal shrinkage, and impaired cell orientation (Fig. S3A). These findings underscore the necessity of actin organization and unidirectional extension for inducing cell arrangement and maintaining orientation. Interestingly, the structure of the bone matrix synthesized by osteoblasts under conditions that

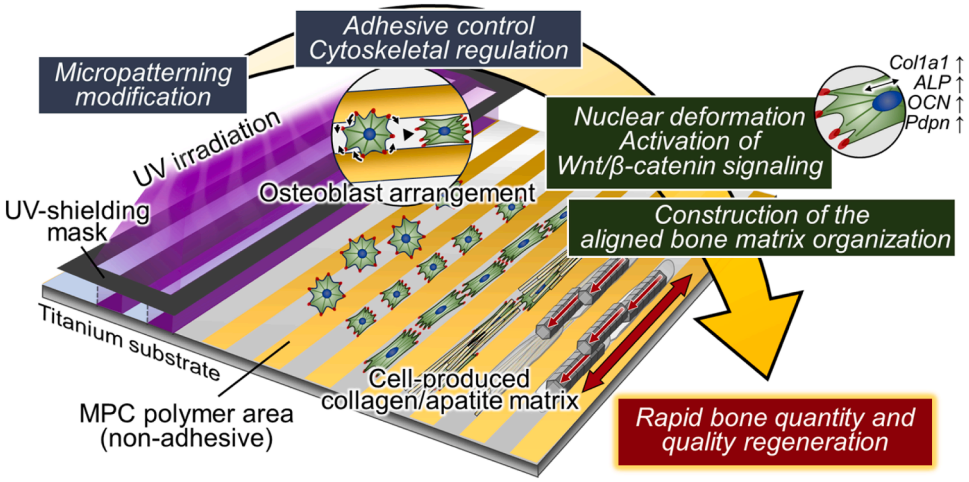

Fig. 8. Schematic of the novel micro-patterned biomaterial for controlling the formation of anisotropic microstructures in bone tissue engineering by distinctly regulating stripe osteoblast adhesion zones. The on/off pattern imposition of cell adhesion on the Ti surface, facilitated by the MPC polymer coating, regulated cell alignment according to width, with the 100 μm pattern inducing the strongest alignment and elongation. Cytoskeletal regulation and nuclear deformation (indicated by the upper right arrowed unidirectional arrow) by this micro-patterned system also modified gene expression, specifically promoting bone differentiation through the activation of the Wnt/β-catenin signaling pathway. Furthermore, osteoblasts aligned and elongated through adhesion regulation induced the formation of a unidirectionally oriented collagen/apatite composite bone matrix (indicated by the bidirectional arrow), similar to the hierarchical organization of natural bone tissue.

repeatedly inhibited actin polymerization was disordered and different from its original structure (Fig. 7A). Osteopetrotic (tl/tl) rats present bones with a disordered collagen/apatite-oriented structure, featuring osteoblasts with fewer, shorter, and maldistributed stress fibers [69]. Although the molecular mechanism underlying bone orientation disruption in this model is not yet understood, it is speculated to result from the lack of coupling between stress fibers and adhesive plaques. Taken together, actin stress fibers in osteoblasts play a crucial role in controlling bone matrix arrangement through the linkage between these fibers and the cell membrane at cell-matrix adhesion sites. Despite osteoblasts showing an enhanced response to oriented substrates with increased canonical Wnt signaling, actin inhibition reduced Wnt signaling to levels equivalent to the unoriented state. These results were supported by quantitative genetic analysis through qPCR, showing decreased β-catenin expression and increased GSK-3β expression due to cytoskeletal inhibition (Fig. 7C). In the absence of Wnt signaling, GSK-3β is thought to phosphorylate and consequently induce β-catenin degradation [70,71]. The elevation in *GSK-3β* levels caused by actin disruption implies increased cytoplasmic degradation and reduced nuclear translocation of β-catenin. The reduced transcriptional activity of β-catenin upon actin inhibition may affect the genetic regulation of genes related to bone matrix orientation. These findings suggest that the parallelization of actin stress fibers in osteoblasts, based on collagen substrate sensing and cytoskeletal regulation, is key to regulating intracellular tension, nuclear shape, and Wnt/β-catenin signaling, ultimately leading to the formation of oriented bone.

Several materials with stripe structures have been developed on Ti substrates to enhance bioactivity. The key advantage of the stripe-micropatterned MPC-Ti in this study is its ability to precisely control cell orientation and flexibility through chemical modification of the adhesive interface. In contrast to the conventional patterned substrates, the present substrate realizes the desired cell extension and induces gene expression alteration through precise control of the adhesive interface. Additionally, this patterning can be applied even after the production of implants from various materials, including CoCr alloys (Fig. S5). Another advantage of this patterned material is its potential to create customizable patterns, as it is fabricated using a photoreaction process. In this study, the effectiveness of linear patterns was demonstrated, while micropatterned MPC-Ti is capable of being designed with customizable crossing angles and dot patterns (Fig. S6), enabling osteogenic tailoring of oriented bone matrix organization that varies depending on the site and patient. In other words, implants with this surface modification pattern are expected to be applicable to any bone location, contributing to the early recovery of bone matrix orientation and, consequently, mechanical function. Based on the above findings, cytoskeletal regulation through stripe-micropatterned MPC-Ti offers a promising approach to rapidly induce bone regeneration in terms of both quantity and quality through orchestrating osteoblast arrangement and activating Wnt/β-catenin signaling.

5. Conclusion

This study presents a novel osteogenic tailoring stripe-micropatterned MPC-Ti for effectively controlling the formation of anisotropic microstructures in bone tissue engineering based on gene expression regulation. The MPC polymer pattern coating imposes an on/off pattern of cell adhesion on the Ti surface, controlling cell arrangement according to width, with the 100 μm pattern inducing the strongest arrangement and elongation. Moreover, cytoskeletal regulation by this micro-patterned substrate altered gene expression, specifically promoting bone differentiation through the activation of the Wnt/β-catenin signaling pathway. Furthermore, the adhesion-controlled osteoblast arrangement and elongation induced the formation of a unidirectionally oriented collagen/apatite composite bone matrix that resembled the hierarchical organization of natural bone tissue. Similarly, osteoblasts on an anisotropic collagen substrate mimicking the biological environment exhibited a strong orientation along the collagen direction and an enhanced Wnt/β-catenin signaling pathway. However, these oriented responses were completely abolished by cytoskeleton inhibition. In summary, we effectively utilized a newly developed micro-patterned biomaterial to artificially control osteoblast orientation and signaling pathways, leading to the formation of anisotropic bone structures, a crucial element in bone functionalization (Fig. 8). This breakthrough holds promise for advancing innovative tissue engineering platforms, promoting functional recovery in bone defects and enhancing the long-term success of bone implants.

CRediT authorship contribution statement

Tadaaki Matsuzaka: Writing – original draft, Visualization,

Methodology, Investigation, Formal analysis. **Aira Matsugaki:** Writing – review & editing, Supervision, Methodology, Formal analysis. **Kazuhiko Ishihara:** Writing – review & editing, Supervision, Methodology, Formal analysis. **Takayoshi Nakano:** Writing – review & editing, Supervision, Project administration, Funding acquisition, Conceptualization.

Declaration of competing interests

The authors declare that they have no known competing financial interests or personal relationships that could have appeared to influence the work reported in this paper.

Data availability statement

Data are available upon request from the corresponding authors.

Acknowledgments

Funding: This work was supported by a Grant-in-Aid for Scientific Research (Grant Number: 24H00382, 23H00235, 22K18310, 21H05197) from the Japan Society for the Promotion of Science (JSPS). This work was partially supported by the Core Research for Evolutional Science and Technology (CREST; Grant Numbers: JPMJCR2194 and JPMJCR22L5) from the Japan Science and Technology Agency (JST).

Supplementary materials

Supplementary material associated with this article can be found, in the online version, at doi:10.1016/j.actbio.2024.12.017.

References

[1] H. Quan, C. Ren, Y. He, F. Wang, S. Dong, H. Jiang, Application of biomaterials in treating early osteonecrosis of the femoral head: research progress and future perspectives, Acta Biomater. 164 (2023) 15–73, https://doi.org/10.1016/j.actbio.2023.04.005.

[2] T. Takizawa, N. Nakayama, H. Haniu, K. Aoki, M. Okamoto, H. Nomura, M. Tanaka, A. Sobajima, K. Yoshida, T. Kamanaka, K. Ajima, A. Oishi, C. Kuroda, H. Ishida, S. Okano, S. Kobayashi, H. Kato, N. Saito, Titanium fiber plates for bone tissue repair, Adv. Mater. 30 (2018) 1703608, https://doi.org/10.1002/adma.201703608.

[3] J. Hou, Z. Xiao, Z. Liu, H. Zhao, Y. Zhu, L. Guo, Z. Zhang, R.O. Ritchie, Y. Wei, X. Deng, An Amorphous Peri-Implant Ligament with Combined Osteointegration and Energy-Dissipation, Adv. Mater. 33 (2021) 2103727, https://doi.org/10.1002/adma.202103727.

[4] N. Ikeo, H. Fukuda, A. Matsugaki, T. Inoue, A. Serizawa, T. Matsuzaka, T. Ishimoto, R. Ozasa, O. Gokcekaya, T. Nakano, 3D puzzle in cube pattern for anisotropic/isotropic mechanical control of structure fabricated by metal additive manufacturing, Crystals 11 (2021) 959, https://doi.org/10.3390/cryst11080959.

[5] L. Salou, A. Hoornaert, G. Louarn, P. Layrolle, Enhanced osseointegration of titanium implants with nanostructured surfaces: an experimental study in rabbits, Acta Biomater. 11 (2015) 494–502, https://doi.org/10.1016/j.actbio.2014.10.017.

[6] M. Fousova, D. Vojtech, E. Jablonska, J. Fojt, J. Lipov, Novel Approach in the Use of Plasma Spray: preparation of Bulk Titanium for Bone Augmentations, Materials 10 (2017) 987, https://doi.org/10.3390/ma10090987.

[7] N. Sirdeshmukh, G. Dongre, Achieving controlled topography and wettability through laser surface texturing of Ti6Al4V for bioengineering applications, Results Eng. 17 (2023) 100898, https://doi.org/10.1016/j.rineng.2023.100898.

[8] L. Bai, P. Chen, Y. Zhao, R. Hang, X. Yao, B. Tang, C. Liu, Y. Xiao, R. Hang, A micro/nano-biomimetic coating on titanium orchestrates osteo/angio-genesis and osteoimmunomodulation for advanced osseointegration, Biomaterials 278 (2021) 121162, https://doi.org/10.1016/j.biomaterials.2021.121162.

[9] Y. Feng, D. Wu, J. Knaus, S. Keßler, B. Ni, Z. Chen, J. Avaro, R. Xiong, H. Cölfen, Z. Wang, A bioinspired gelatin–amorphous calcium phosphate coating on titanium implant for bone regeneration, Adv. Healthc. Mater. 12 (2023) 2203411, https://doi.org/10.1002/adhm.202203411.

[10] A. Hariharan, P. Goldberg, F. Schell, U. Hempel, F. Striggow, M. Hantusch, M. Medina-Sánchez, A.F. Lasagni, A. Gebert, Single- and multiscale laser patterning of 3D printed biomedical titanium alloy: toward an enhanced adhesion and early differentiation of human bone marrow stromal cells, Adv. Funct. Mater. 34 (2023) 2310607, https://doi.org/10.1002/adfm.202310607.

[11] S. Wang, X. Zhao, Y. Hsu, Y. He, F. Wang, F. Yang, F. Yan, D. Xia, Y. Liu, Surface modification of titanium implants with Mg-containing coatings to promote osseointegration, Acta Biomater. 169 (2023) 19–44, https://doi.org/10.1016/j.actbio.2023.07.048.

[12] N. Khuu, S. Kheiri, E. Kumacheva, Structurally anisotropic hydrogels for tissue engineering, Trends Chem. 3 (2021) 1002–1026, https://doi.org/10.1016/j.trechm.2021.09.009.

[13] T. Nakano, K. Kaibara, T. Ishimoto, Y. Tabata, Y. Umakoshi, Biological apatite (BAp) crystallographic orientation and texture as a new index for assessing the microstructure and function of bone regenerated by tissue engineering, Bone 51 (2012) 741–747, https://doi.org/10.1016/j.bone.2012.07.003.

[14] C. Ma, T. Du, X. Niu, Y. Fan, Biomechanics and mechanobiology of the bone matrix, Bone Res. 10 (2022) 1–17, https://doi.org/10.1038/s41413-022-00223-y.

[15] W.J. Landis, The strength of a calcified tissue depends in part on the molecular structure and organization of its constituent mineral crystals in their organic matrix, Bone 16 (1995) 533–544, https://doi.org/10.1016/8756-3282(95)00076-P.

[16] T. Nakano, K. Kaibara, Y. Tabata, N. Nagata, S. Enomoto, E. Marukawa, Y. Umakoshi, Unique alignment and texture of biological apatite crystallites in typical calcified tissues analyzed by microbeam x-ray diffractometer system, Bone 31 (2002) 479–487, https://doi.org/10.1016/S8756-3282(02)00850-5.

[17] J. Wang, T. Ishimoto, T. Nakano, Unloading-induced degradation of the anisotropic arrangement of collagen/apatite in rat femurs, Calcif. Tissue Int. 100 (2017) 87–94, https://doi.org/10.1007/s00223-016-0200-0.

[18] J. Wang, T. Ishimoto, T. Matsuzaka, A. Matsugaki, R. Ozasa, T. Matsumoto, M. Hayashi, H.S. Kim, T. Nakano, Adaptive enhancement of apatite crystal orientation and Young's modulus under elevated load in rat ulnar cortical bone, Bone 181 (2024) 117024, https://doi.org/10.1016/j.bone.2024.117024.

[19] T. Ishimoto, T. Nakano, Y. Umakoshi, M. Yamamoto, Y. Tabata, Degree of biological apatite c-axis orientation rather than bone mineral density controls mechanical function in bone regenerated using recombinant bone morphogenetic protein-2, J. Bone Miner. Res. 28 (2013) 1170–1179, https://doi.org/10.1002/jbmr.1825.

[20] Y. Noyama, T. Nakano, T. Ishimoto, T. Sakai, H. Yoshikawa, Design and optimization of the oriented groove on the hip implant surface to promote bone microstructure integrity, Bone 52 (2013) 659–667, https://doi.org/10.1016/j.bone.2012.11.005.

[21] T. Matsuzaka, A. Matsugaki, T. Nakano, Control of osteoblast arrangement by osteocyte mechanoresponse through prostaglandin E2 signaling under oscillatory fluid flow stimuli, Biomaterials 279 (2021) 121203, https://doi.org/10.1016/j.biomaterials.2021.121203.

[22] A. Matsugaki, T. Matsuzaka, T. Mori, M. Saito, K. Funaoku, R. Yamano, O. Gokcekaya, R. Ozasa, T. Nakano, PBF-LB fabrication of microgrooves for induction of osteogenic differentiation of hMSCs, Int. J. Bioprinting 10 (2023) 1425, https://doi.org/10.36922/ijb.1425.

[23] A. Matsugaki, Y. Isobe, T. Saku, T. Nakano, Quantitative regulation of bone-mimetic, oriented collagen/apatite matrix structure depends on the degree of osteoblast alignment on oriented collagen substrates, J. Biomed. Mater. Res. A 103 (2015) 489–499, https://doi.org/10.1002/jbm.a.35189.

[24] A. Matsugaki, N. Fujiwara, T. Nakano, Continuous cyclic stretch induces osteoblast alignment and formation of anisotropic collagen fiber matrix, Acta Biomater. 9 (2013) 7227–7235, https://doi.org/10.1016/j.actbio.2013.03.015.

[25] A. Matsugaki, G. Aramoto, T. Nakano, The alignment of MC3T3-E1 osteoblasts on steps of slip traces introduced by dislocation motion, Biomaterials 33 (2012) 7327–7335, https://doi.org/10.1016/j.biomaterials.2012.06.022.

[26] A. Matsugaki, G. Aramoto, T. Ninomiya, H. Sawada, S. Hata, T. Nakano, Abnormal arrangement of a collagen/apatite extracellular matrix orthogonal to osteoblast alignment is constructed by a nanoscale periodic surface structure, Biomaterials 37 (2015) 134–143, https://doi.org/10.1016/j.biomaterials.2014.10.025.

[27] Y. Nakanishi, A. Matsugaki, K. Kawahara, T. Ninomiya, H. Sawada, T. Nakano, Unique arrangement of bone matrix orthogonal to osteoblast alignment controlled by Tspan11-mediated focal adhesion assembly, Biomaterials 209 (2019) 103–110, https://doi.org/10.1016/j.biomaterials.2019.04.016.

[28] S. Lee, A. Matsugaki, T. Kasuga, T. Nakano, Development of bifunctional oriented bioactive glass/poly(lactic acid) composite scaffolds to control osteoblast alignment and proliferation, J. Biomed. Mater. Res. A 107 (2019) 1031–1041, https://doi.org/10.1002/jbm.a.36619.

[29] F.R. Valencia, E. Sandoval, J. Du, E. Iu, J. Liu, S.V. Plotnikov, Force-dependent activation of actin elongation factor mDia1 protects the cytoskeleton from mechanical damage and promotes stress fiber repair, Dev. Cell 56 (2021), https://doi.org/10.1016/j.devcel.2021.11.004, 3288–3302.e5.

[30] A. Matsugaki, D. Yamazaki, T. Nakano, Selective patterning of netrin-1 as a novel guiding cue for anisotropic dendrogenesis in osteocytes, Mater. Sci. Eng. C 108 (2020) 110391, https://doi.org/10.1016/j.msec.2019.110391.

[31] N.S. Kalson, T. Starborg, Y. Lu, A. Mironov, S.M. Humphries, D.F. Holmes, K. E. Kadler, Nonmuscle myosin II powered transport of newly formed collagen fibrils at the plasma membrane, Proc. Natl. Acad. Sci. 110 (2013) E4743–E4752, https://doi.org/10.1073/pnas.1314348110.

[32] R. Watanabe, A. Matsugaki, O. Gokcekaya, R. Ozasa, T. Matsumoto, H. Takahashi, H. Yasui, T. Nakano, Host bone microstructure for enhanced resistance to bacterial infections, Biomater. Adv. 154 (2023) 213633, https://doi.org/10.1016/j.bioadv.2023.213633.

[33] K. Fukazawa, Q. Li, S. Seeger, K. Ishihara, Direct observation of selective protein capturing on molecular imprinting substrates, Biosens. Bioelectron. 40 (2013) 96–101, https://doi.org/10.1016/j.bios.2012.06.033.

[34] K. Fukazawa, K. Ishihara, Synthesis of photoreactive phospholipid polymers for use in versatile surface modification of various materials to obtain extreme wettability, ACS Appl. Mater. Interfaces 5 (2013) 6832–6836, https://doi.org/10.1021/am402051e.

[35] J. Choi, T. Konno, R. Matsuno, M. Takai, K. Ishihara, Surface immobilization of biocompatible phospholipid polymer multilayered hydrogel on titanium alloy, Colloids Surf. B Biointerfaces 67 (2008) 216–223, https://doi.org/10.1016/j.colsurfb.2008.08.025.
[36] J.E. Kirkwood, G.G. Fuller, Liquid crystalline collagen: a self-assembled morphology for the orientation of mammalian cells, Langmuir 25 (2009) 3200–3206, https://doi.org/10.1021/la803736x.
[37] Y. Kimura, A. Matsugaki, A. Sekita, T. Nakano, Alteration of osteoblast arrangement via direct attack by cancer cells: new insights into bone metastasis, Sci. Rep. 7 (2017) 44824, https://doi.org/10.1038/srep44824.
[38] M. Janko, P. Davydovskaya, M. Bauer, A. Zink, R.W. Stark, Anisotropic Raman scattering in collagen bundles, Opt. Lett. 35 (2010) 2765–2767, https://doi.org/10.1364/OL.35.002765.
[39] J.R. Ferraro, K. Nakamoto, C.W. Brown, Introductory Raman Spectroscopy, Elsevier, 2003, https://doi.org/10.1016/B978-0-12-254105-6.X5000-8.
[40] A. Masic, L. Bertinetti, R. Schuetz, L. Galvis, N. Timofeeva, J.W.C. Dunlop, J. Seto, M.A. Hartmann, P. Fratzl, Observations of Multiscale, Stress-induced changes of collagen orientation in tendon by polarized Raman spectroscopy, Biomacromolecules 12 (2011) 3989–3996, https://doi.org/10.1021/bm201008b.
[41] K. Ishihara, Revolutionary advances in 2-methacryloyloxyethyl phosphorylcholine polymers as biomaterials, J. Biomed. Mater. Res. A 107 (2019) 933–943, https://doi.org/10.1002/jbm.a.36635.
[42] F. Xing, H. Zhang, M. Li, H. Dong, X. Ma, S. Deng, F. Hu, I. Lee, L. Pan, J. Xu, Regulation of actin cytoskeleton via photolithographic micropatterning, J. Innov. Opt. Health Sci. 16 (2023) 2244005, https://doi.org/10.1142/S1793545822440059.
[43] V. Maruthamuthu, Y. Aratyn-Schaus, M.L. Gardel, Conserved F-actin dynamics and force transmission at cell adhesions, Curr. Opin. Cell Biol. 22 (2010) 583–588, https://doi.org/10.1016/j.ceb.2010.07.010.
[44] S. Fusco, V. Panzetta, V. Embrione, P.A. Netti, Crosstalk between focal adhesions and material mechanical properties governs cell mechanics and functions, Acta Biomater 23 (2015) 63–71, https://doi.org/10.1016/j.actbio.2015.05.008.
[45] G. Gronowicz, M.B. McCarthy, Response of human osteoblasts to implant materials: integrin-mediated adhesion, J. Orthop. Res. 14 (1996) 878–887, https://doi.org/10.1002/jor.1100140606.
[46] C.Y. Yang, W.Y. Huang, L.H. Chen, N.W. Liang, H.C. Wang, J. Lu, X. Wang, T. W. Wang, Neural tissue engineering: the influence of scaffold surface topography and extracellular matrix microenvironment, J. Mater. Chem. B 9 (2021) 567–584, https://doi.org/10.1039/D0TB01605E.
[47] R. Joshi, S.B. Han, W.K. Cho, D.H. Kim, The role of cellular traction forces in deciphering nuclear mechanics, Biomater. Res. 26 (2022) 43, https://doi.org/10.1186/s40824-022-00289-z.
[48] J. Sun, J. Chen, K. Amar, Y. Wu, M. Jiang, N. Wang, LAP2β transmits force to upregulate genes via chromatin domain stretching but not compression, Acta Biomater 163 (2023) 326–338, https://doi.org/10.1016/j.actbio.2021.10.029.
[49] S.H. Lim, X.Y. Liu, H. Song, K.J. Yarema, H.Q. Mao, The effect of nanofiber-guided cell alignment on the preferential differentiation of neural stem cells, Biomaterials 31 (2010) 9031–9039, https://doi.org/10.1016/j.biomaterials.2010.08.021.
[50] C.X. Song, S.Y. Liu, W.T. Zhu, S.Y. Xu, G.X. Ni, Excessive mechanical stretch-mediated osteoblasts promote the catabolism and apoptosis of chondrocytes via the Wnt/β-catenin signaling pathway, Mol. Med. Rep. 24 (2021) 1–10, https://doi.org/10.3892/mmr.2021.12232.
[51] J. Zhu, X. Zhang, C. Wang, X. Peng, X. Zhang, Different magnitudes of tensile strain induce human osteoblasts differentiation associated with the activation of ERK1/2 phosphorylation, Int. J. Mol. Sci. 9 (2008) 2322–2332, https://doi.org/10.3390/ijms9122322.
[52] M. Ponzetti, N. Rucci, Osteoblast differentiation and signaling: established concepts and emerging topics, Int. J. Mol. Sci. 22 (2021) 6651, https://doi.org/10.3390/ijms22136651.
[53] L. Feng, J. Zhang, L. Shi, Z. Yang, T. Wu, H. Wang, W. Lin, Y. Lu, J.H.T. Lo, D. Zhu, G. Li, MicroRNA-378 Suppressed Osteogenesis of MSCs and Impaired Bone Formation via Inactivating Wnt/β-Catenin Signaling, Mol. Ther. Nucleic Acids 21 (2020) 1017–1028, https://doi.org/10.1016/j.omtn.2020.07.018.
[54] D.S. Amarasekara, S. Kim, J. Rho, Regulation of osteoblast differentiation by cytokine networks, Int. J. Mol. Sci. 22 (2021) 2851, https://doi.org/10.3390/ijms22062851.
[55] S. Goel, E.N. Chin, S.A. Fakhraldeen, S.M. Berry, D.J. Beebe, C.M. Alexander, Both LRP5 and LRP6 receptors are required to respond to physiological wnt ligands in mammary epithelial cells and fibroblasts, J. Biol. Chem. 287 (2012) 16454–16466, https://doi.org/10.1074/jbc.M112.362137.
[56] B.T. MacDonald, K. Tamai, X. He, Wnt/β-catenin signaling: components, mechanisms, and diseases, Dev. Cell 17 (2009) 9–26, https://doi.org/10.1016/j.devcel.2009.06.016.
[57] T. Gaur, C.J. Lengner, H. Hovhannisyan, R.A. Bhat, P.V.N. Bodine, B.S. Komm, A. Javed, A.J. van Wijnen, J.L. Stein, G.S. Stein, J.B. Lian, Canonical wnt signaling promotes osteogenesis by directly stimulating Runx2 gene expression, J. Biol. Chem. 280 (2005) 33132–33140, https://doi.org/10.1074/jbc.M500608200.
[58] A. Akiva, J. Melke, S. Ansari, N. Liv, R. van der Meijden, M. van Erp, F. Zhao, M. Stout, W.H. Nijhuis, C. de Heus, C. Muñiz Ortera, J. Fermie, J. Klumperman, K. Ito, N. Sommerdijk, S. Hofmann, An organoid for woven bone, Adv. Funct. Mater. 31 (2021) 2010524, https://doi.org/10.1002/adfm.202010524.
[59] G.J. Spencer, J.C. Utting, S.L. Etheridge, T.R. Arnett, P.G. Genever, Wnt signalling in osteoblasts regulates expression of the receptor activator of NFκB ligand and inhibits osteoclastogenesis in vitro, J. Cell Sci. 119 (2006) 1283–1296, https://doi.org/10.1242/jcs.02883.
[60] Y.-W. Qiang, Y. Chen, O. Stephens, N. Brown, B. Chen, J. Epstein, B. Barlogie, J. D. Shaughnessy, Myeloma-derived Dickkopf-1 disrupts Wnt-regulated osteoprotegerin and RANKL production by osteoblasts: a potential mechanism underlying osteolytic bone lesions in multiple myeloma, Blood 112 (2008) 196–207, https://doi.org/10.1182/blood-2008-01-132134.
[61] T. Ishimoto, K. Kawahara, A. Matsugaki, H. Kamioka, T. Nakano, Quantitative evaluation of osteocyte morphology and bone anisotropic extracellular matrix in rat femur, Calcif. Tissue Int. 109 (2021) 434–444, https://doi.org/10.1007/s00223-021-00852-1.
[62] T. Ishimoto, Y. Kobayashi, M. Takahata, M. Ito, A. Matsugaki, H. Takahashi, R. Watanabe, T. Inoue, T. Matsuzaka, R. Ozasa, T. Hanawa, K. Yokota, Y. Nakashima, T. Nakano, Outstanding in vivo mechanical integrity of additively manufactured spinal cages with a novel “honeycomb tree structure” design via guiding bone matrix orientation, Spine J 22 (2022) 1742–1757, https://doi.org/10.1016/j.spinee.2022.05.006.
[63] A. Matsugaki, M. Ito, Y. Kobayashi, T. Matsuzaka, R. Ozasa, T. Ishimoto, H. Takahashi, R. Watanabe, T. Inoue, K. Yokota, Y. Nakashima, T. Kaito, S. Okada, T. Hanawa, Y. Matsuyama, M. Matsumoto, H. Taneichi, T. Nakano, Innovative design of bone quality-targeted intervertebral spacer: accelerated functional fusion guiding oriented collagen and apatite microstructure without autologous bone graft, Spine J 23 (2023) 609–620, https://doi.org/10.1016/j.spinee.2022.12.011.
[64] S. Kakinoki, J.-H. Seo, Y. Inoue, K. Ishihara, N. Yui, T. Yamaoka, Mobility of the Arg-Gly-Asp ligand on the outermost surface of biomaterials suppresses integrin-mediated mechanotransduction and subsequent cell functions, Acta Biomater 13 (2015) 42–51, https://doi.org/10.1016/j.actbio.2014.11.020.
[65] N.R. Gould, O.M. Torre, J.M. Leser, J.P. Stains, The cytoskeleton and connected elements in bone cell mechano-transduction, Bone 149 (2021) 115971, https://doi.org/10.1016/j.bone.2021.115971.
[66] K. Ohashi, S. Fujiwara, K. Mizuno, Roles of the cytoskeleton, cell adhesion and rho signalling in mechanosensing and mechanotransduction, J. Biochem. 161 (2017) 245–254, https://doi.org/10.1093/jb/mvw082.
[67] W. Shi, Y. Xie, J. He, J. Zhou, Y. Gao, W. Wei, N. Ding, H. Ma, C.J. Xian, K. Chen, J. Wang, Microgravity induces inhibition of osteoblastic differentiation and mineralization through abrogating primary cilia, Sci. Rep. 7 (2017) 1866, https://doi.org/10.1038/s41598-017-02049-9.
[68] J. Kim, T. Adachi, Cell-fate decision of mesenchymal stem cells toward osteocyte differentiation is committed by spheroid culture, Sci. Rep. 11 (2021) 13204, https://doi.org/10.1038/s41598-021-92607-z.
[69] J.W. Lee, T. Nakano, S. Toyosawa, Y. Tabata, Y. Umakoshi, Areal distribution of preferential alignment of biological apatite (BAp) crystallite on cross-section of center of femoral diaphysis in osteopetrotic (op/op) mouse, Mater. Trans. 48 (2007) 337–342, https://doi.org/10.2320/matertrans.48.337.
[70] N. AlMuraikhi, S. Binhamdan, H. Alaskar, A. Alotaibi, S. Tareen, M. Muthurangan, M. Alfayez, Inhibition of GSK-3β enhances osteoblast differentiation of human mesenchymal stem cells through wnt signaling overexpressing Runx2, Int. J. Mol. Sci. 24 (2023) 7164, https://doi.org/10.3390/ijms24087164.
[71] E.Y. Chen, M.T. DeRan, M.S. Ignatius, K.B. Grandinetti, R. Clagg, K.M. McCarthy, R.M. Lobbardi, J. Brockmann, C. Keller, X. Wu, D.M. Langenau, Glycogen synthase kinase 3 inhibitors induce the canonical WNT/β-catenin pathway to suppress growth and self-renewal in embryonal rhabdomyosarcoma, Proc. Natl. Acad. Sci. 111 (2014) 5349–5354, https://doi.org/10.1073/pnas.1317731111.